Passive vibration control using a metaconcrete thin plate

E. J. P. Miranda Jr.[1]*, A. F. Angelin[2], F. M. Silva[2], J. M. C. Dos Santos[3]
[1]Federal Institute of Maranhão, EIB-DE, R. Afonso Pena 174, 65010-030, São Luís, MA, Brazil
[2]University of Campinas, FT, Limeira, SP, Brazil
[3]University of Campinas, FEM-DMC, Campinas, SP, Brazil

Abstract

We investigated the band structure of flexural waves propagating in a metaconcrete thin plate, consisting of a concrete matrix reinforced by steel inclusions coated by rubber in square and triangular lattices. We considered the classical Kirchhoff-Love thin plate theory. We also studied the influence of inclusion geometry - circular, square and rotated square with a 45° angle of rotation with respect to the x, y axes. Improved plane wave expansion method was used to solve the wave equation considering flexural wave propagation in the xy plane. Flat bands and locally resonant band gaps were observed for all types of inclusion studied regarding square and triangular lattices. The locally resonant band gaps for square and rotated square inclusions in a triangular lattice were slightly shifted to higher frequencies than that given by circular inclusion. We suggest that the metaconcrete thin plate studied should be feasible for flexural vibration control in low frequencies.
Keywords: metaconcrete, thin plate theory, locally resonant band gaps, flexural vibration control, improved plane wave expansion method.

INTRODUCTION

Phononic crystals (PnCs) are artificial composites consisting of periodic arrays of inclusions embedded in a matrix. They have received renewed attention since they exhibit band gaps, which are ranges of frequency, where there are no mechanical (elastic or acoustic) propagating waves. There are only evanescent Bloch waves within the band gaps. The physical origin of phononic and photonic band gaps can be understood at micro-scale using the classical wave theory to describe Bragg and Mie resonances based on the scattering of mechanical and electromagnetic waves propagating within the crystal [1]. The formation of phononic band gaps is based on the Bragg scattering mechanism, whose frequency location is given by Bragg's law, i.e., $a=n(\lambda/2)$ ($n \in \mathbb{N}_{>0}$), where a is the lattice parameter and λ is the wavelength in the host material. From Bragg's law, one can observe that it is not possible to open up Bragg-type band gaps in low-frequencies for small size PnCs. In order to overcome this issue, Liu and co-workers [2] proposed a locally resonant phononic crystal (LRPnC), also known as mechanical (elastic or acoustic) metamaterial, consisting of arrays of localized resonant structures. These resonance-type band gaps, also known as locally resonant band gaps (LRBGs), were obtained in a frequency range two orders of magnitude lower than that given by the Bragg's limit. LRBGs arise on the vicinity of resonator natural frequency and they do not depend on periodicity, whereas Bragg-type band gaps typically occur at wavelengths of the order of unit cell size and depend on periodicity.

Mechanical metamaterials (MMs) have been extensively applied in the last years as harnessed shape morphing [3], topological protection [4], sustainable metamaterials [5], acoustic barriers [6], vibration isolators [7], among others. A new type of MM called metaconcrete has also been investigated in the last few years [8-13]. This expression, i.e., metaconcrete, was used first by Mitchell and co-workers [10]. They [10] proposed a new type of concrete for the attenuation of elastic waves using the concept of LRBGs. The traditional aggregates, for instance, stone, sand and gravel, were replaced with spherical inclusions consisting of a heavy metal core coated with a soft outer layer. They observed that the inclusions are able to absorb a significant portion of the applied energy. Cheng and Shi [9] investigated the attenuation zones of two-dimensional (2D) periodic rubber concrete panels, considering both Bragg-type and LRBGs. They remarked that non-symmetric panels with directional attenuation zones are much suitable for engineering applications. Moreover, they observed that the vibration can be reduced significantly by using a periodic structure with only three units. Miniaci et al. [13] proposed a novel approach in order to handle seismic events. They discussed the feasibility of a passive isolation strategy for seismic waves based on large-scale MMs. They remarked that both surface and bulk seismic waves can be considerably attenuated, thus their proposed strategy is viable for the protection of civil structures against seismic risk [13].

Most studies about metaconcrete focused only on the band structure of bulk waves propagating in a solid with infinite thickness and did not investigate the band structure of flexural waves in a thin plate. The main purpose of this study is to investigate the elastic band structure, also known as dispersion diagram, of a metaconcrete thin plate

*edson.jansen@ifma.edu.br
https://orcid.org/0000-0003-1100-9169

composed of steel inclusions coated by rubber embedded in a concrete matrix. The wave propagation in the xy plane (only flexural vibration is considered) and the classical Kirchhoff-Love [14, 15] thin plate theory are regarded. The metaconcrete thin plate has 2D periodicity, different inclusion cross sections - circular, square and rotated square with a 45° angle of rotation with respect to the x, y axes, and different lattices - square and triangular. The semi-analytical improved plane wave expansion (IPWE) [16, 17] method is used to calculate the band structure. LRBGs are observed for all types of inclusion regarding both square and triangular lattices. The paper is organized as follows. The 2nd section presents IPWE approach for the metaconcrete thin plate. In the following, i.e., 3rd section, simulated examples were carried out. We analyzed the LRBGs considering just the propagating modes obtained by IPWE method in the first Brillouin zone (FBZ) [18].

METACONCRETE THIN PLATE MODELLING

Figs. 1a and 1b sketch the cross section of a 2D elastic metaconcrete thin plate with square and triangular lattices and arbitrary inclusions. Figs. 1c and 1d show the FBZ of both square and triangular lattices. Fig. 2 shows as example the actual 2D elastic metaconcrete thin plate with square lattice (a) and its unit cell (b). The inclusions of the metaconcrete thin plate are illustrated in Fig. 3. They had circular (a), square (b) and rotated square with a 45° angle of rotation with respect to the x, y axes (c) geometries and they were composed by steel inclusions (grey) coated by rubber (black) embedded in a concrete matrix.

Improved plane wave expansion: this subsection presents the IPWE formulation for the metaconcrete thin plate using IPWE, also known as ω(k) approach, where ω is the angular frequency and k is the Bloch wave vector, also known as wave number, based on the classical elasticity theory. We regarded 2D periodicity (Fig. 1), isotropic thin plate and flexural wave

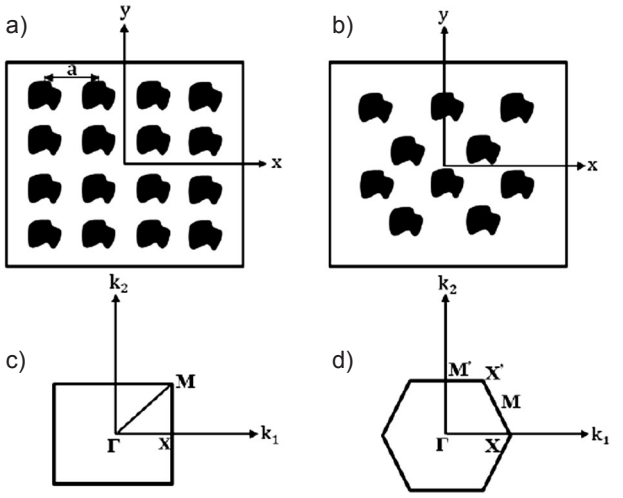

Figure 1: Transverse cross section of the metaconcrete thin plate: an array of inclusions periodically distributed in a concrete matrix, considering square (a) and triangular (b) lattices. First Brillouin zone for square (c) and triangular (d) lattices.

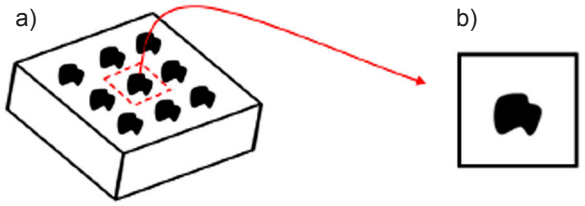

Figure 2: Illustration of the metaconcrete thin plate with inclusions periodically distributed in a concrete matrix, considering square lattice (a) and its unit cell (b).

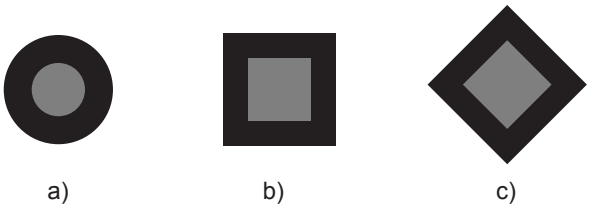

Figure 3: Transverse cross section of the metaconcrete thin plate inclusions: a) circular; b) square; and c) rotated square with a 45° angle of rotation with respect to the x, y axes.

propagation in the xy plane. Plane wave expansion (PWE) is one of the most used methods to calculate the band structure of PnCs and it has also been employed to calculate the band structure of elastic metamaterials [19]. However, when there is a high geometry or material mismatch PWE presents slow convergence and IPWE must be used [17]. From Kirchhoff-Love theory [14, 15], the governing equation for flexural vibration of a uniform thin plate in the absence of body forces is [20]:

$$-\alpha\frac{\partial^2 w(r,t)}{\partial t^2}=\frac{\partial^2}{\partial x^2}\left[D\frac{\partial^2 w(r,t)}{\partial x^2}+\beta\frac{\partial^2 w(r,t)}{\partial y^2}\right]+2\frac{\partial^2}{\partial x\partial y}\left[\gamma\frac{\partial^2 w(r,t)}{\partial x\partial y}\right]+\frac{\partial^2}{\partial y^2}\left[D\frac{\partial^2 w(r,t)}{\partial y^2}+\beta\frac{\partial^2 w(r,t)}{\partial x^2}\right] \quad (A)$$

where t is time, $D=Eh^3/[12(1-\nu^2)]$ is the bending stiffness, E is the Young's modulus, ν is the Poisson's ratio, h is the thickness, ρ is the density, $\alpha=\rho h$, $\beta=D\nu$, and $\gamma=D(1-\nu)$. For a 2D periodicity the system has translational symmetry in z direction and the material parameters depend only on the x and y coordinates, then $r=xe_1+ye_2$ $(x,y\in\mathbb{R})$ is the 2D spatial vector, where e_i (i=1,2) are the basis vectors in the real space and w(r,t) is the transverse displacement in z direction (out of plane). An appropriate condition for the validity of thin plate theory is $h<\lambda/6$ [21] and/or $k_p h<<1$, $h/a<<1$ [22], with $\lambda=2\pi/k_p$, where $k_p=(\rho\omega^2/D)^{1/4}$ is the flexural wave number of the thin plate. Applying the temporal Fourier transform to Eq. A and omitting frequency dependence results in:

$$\omega^2\alpha w(r)=\frac{\partial^2}{\partial x^2}\left[D\frac{\partial^2 w(r)}{\partial x^2}+\beta\frac{\partial^2 w(r)}{\partial y^2}\right]+2\frac{\partial^2}{\partial x\partial y}\left[\gamma\frac{\partial^2 w(r)}{\partial x\partial y}\right]+\frac{\partial^2}{\partial y^2}\left[D\frac{\partial^2 w(r)}{\partial y^2}+\beta\frac{\partial^2 w(r)}{\partial x^2}\right] \quad (B)$$

In addition, considering a metaconcrete thin plate, one can note that $\alpha=\alpha(r)$, $D=D(r)$, $\beta=\beta(r)$ and $\gamma=\gamma(r)$ because we considered three different materials - steel inclusions coated with rubber and a concrete matrix, and $w(r)=w(r,\omega)$. Applying the Floquet-Bloch's theorem [23, 24], expanding Bloch wave amplitude as Fourier series in reciprocal space and considering wave propagation in the xy plane ($k_3=0$), we can write:

$$w(r)=e^{jk.r}w_k(r)=e^{jk.r}\sum_{g=-\infty}^{+\infty} w(g)e^{jg.r}=\sum_{g=-\infty}^{+\infty} w(r)e^{j(k+g).r} \quad (C)$$

where $j=\sqrt{-1}$ and $w_k(r)$ is the Bloch wave amplitude. Note that $w_k(r)=w_k(r+\bar{r})$ and $w(r+\bar{r})=w(r)e^{jk.\bar{r}}$, where $e^{jk.\bar{r}}$ is called the Floquet-Bloch periodic boundary condition, $k=\bar{u}b_1+\bar{v}b_2$, $\bar{u}$, $\bar{v} \in \mathbb{Q}$ are the symmetry points within the FBZ in reciprocal space or we may write $k=k_1e_1+k_2e_2$, $k_1, k_2 \in \mathbb{R}$ are the point coordinates within the FBZ in Figs. 1c and 1d for the reciprocal space. The basis vectors in reciprocal space b_i ($i=1,2$) are defined as $a_i.b_j=2\pi\delta_{ij}$, $\delta_{ij}=0$ if $i\neq j$ or $\delta_{ij}=1$ if $i=j$ is the Kronecker delta, $b_1=2\pi(a_2\times a_3)/[a_1.(a_2\times a_3)]$, $b_2=2\pi(a_3\times a_1)/[a_2.(a_3\times a_1)]$, a_i ($i=1,2$) are the components of the lattice vector $\bar{r}=(\bar{p}a_1+\bar{q}a_2)$ ($\bar{p}, \bar{q} \in \mathbb{Z}$).

The lattice vector components for a square lattice are $a_i=ae_j$ ($i=1,2$) and for triangular lattice are $a_1=ae_1$, $a_2=(a/2)e_1+(a\sqrt{3}/2)e_2$. The reciprocal lattice vector is defined as $g=(2\pi/a)(me_1+ne_2)$ ($m,n \in \mathbb{Z}$) for square lattice and $g=(2\pi/a)\{me_1+[(-m+2n)/\sqrt{3}]e_2\}$ for triangular lattice. Note that g is a 2D vector because we consider 2D periodicity. Furthermore, we may expand $\alpha(r)$, $1/D(r)$, $1/\beta(r)$ and $1/\gamma(r)$ in Fourier series on the reciprocal space as:

$$P(r)=\sum_{\bar{g}=-\infty}^{+\infty} P(\bar{g})e^{j\bar{g}.r} \quad (D)$$

where $P(r)$ is one of the $\alpha(r)$, $1/D(r)$, $1/\beta(r)$ and $1/\gamma(r)$, and $\bar{g}$ has the same expressions of g with $\bar{m}, \bar{n} \in \mathbb{Z}$. We used $\bar{g}$ instead of g to highlight the difference between the Fourier series expansion of material properties and Bloch wave amplitude. The Fourier series coefficients, $P(\bar{g})$, are reported in [25], considering different lattices and inclusion cross sections. The inclusions in [25] are composed of one material. In addition, the Fourier series coefficients for PnC inclusions with two materials are described in [26]. Substituting Eqs. C and D in Eq. B, with $\tilde{g}=\bar{g}+g$, multiplying by $e^{-j\bar{g}.r}$ and integrating over the unit cell, we may write:

$$\begin{aligned}&\sum_{g=-\infty}^{+\infty}\Big\{-\omega^2\alpha(\bar{g}-g)+\left[\frac{1}{D(\bar{g}-g)}\right]^{-1}(k+g)_1^2\,(k+\bar{g})_1^2+\left[\frac{1}{\beta(\bar{g}-g)}\right]^{-1}\\&(k+g)_2^2\,(k+\bar{g})_1^2+2\left[\frac{1}{\gamma(\bar{g}-g)}\right]^{-1}(k+g)_2(k+g)_1(k+\bar{g})_2(k+\bar{g})_1\\&+\left[\frac{1}{D(\bar{g}-g)}\right]^{-1}(k+g)_2^2\,(k+\bar{g})_2^2+\left[\frac{1}{\beta(\bar{g}-g)}\right]^{-1}(k+g)_1^2\,(k+\bar{g})_2^2\Big\}w(g)=0\end{aligned} \quad (E)$$

Eq. E is an infinite system of equations, thus we truncated the Fourier series, i.e. $m,\bar{m},n,\bar{n}=[-M, \ldots, M]$ ($M \in \mathbb{N}_{>0}$), and the total number of plane waves was $(2M+1)^2$. Eq. E represents a generalized eigenvalue problem of $\omega^2(k)$ and was solved for each k into the FBZ for square and triangular lattices (Figs. 1c and 1d). Eq. E can be expressed in a matrix form as:

$$(K-\omega^2M)w=0 \quad (F)$$

where

$$\begin{aligned}&K=(\overline{K}+G)_1^2\left[\frac{1}{D}\right]^{-1}(\overline{K}+\overline{G})_1^2+(\overline{K}+G)_2^2\left[\frac{1}{B}\right]^{-1}(\overline{K}+\overline{G})_1^2+2(\overline{K}+G)_2\\&(\overline{K}+G)_1\left[\frac{1}{\Gamma}\right]^{-1}(\overline{K}+\overline{G})_2\,(\overline{K}+\overline{G})_1+(\overline{K}+G)_2^2\left[\frac{1}{D}\right]^{-1}\\&(\overline{K}+\overline{G})_2^2+(\overline{K}+G)_1^2\left[\frac{1}{B}\right]^{-1}(\overline{K}+\overline{G})_2^2\end{aligned} \quad (G)$$

$$M=P(\bar{g}-g)h \quad (H)$$

$$w=w(g)=\{w[g(-M,-M)]w[g(-M+1,-M+1)]...w[g(M,M)]\}^T \quad (I)$$

The form of matrices $\overline{K}$, G, $\overline{G}$, $[1/D]^{-1}$, $[1/B]^{-1}$, $[1/\Gamma]^{-1}$ and $P(\bar{g}-g)$ has already been addressed in [27].

SIMULATED EXAMPLES

The physical parameters of rubber (A), steel (B) and concrete (C) are listed in Table I. The material properties described were obtained from [28]. The filling fractions in Table I were defined as $\bar{f}_1=S_A/S_C$ and $\bar{f}_2=S_B/S_C$, where S_A, S_B, and S_C are the cross-section areas of the coating (rubber), considering it filled, core (steel), and unit cell, respectively. The filling fractions for square and triangular lattices are addressed in [25]. It can be observed from Table I that the coating rubber has very small Young's modulus, i.e., very small elastic constants, and consequently very low sound propagation velocity. This is the basic condition for the existence of local resonances, since it facilitates the vibration of the steel core inclusions [29].

Table I - Physical parameters of rubber (A), steel (B) and concrete (C).

Geometry/Property	Value
Lattice parameter, a (m)	0.03
Thickness, h (m)	0.003
Filling fraction, $\bar{f}_1$	0.335
Filling fraction, $\bar{f}_2$	0.335/6
Mass density, ϱ_A, ϱ_B, ϱ_C (kg/m^3)	1300, 7890, 2500
Young's modulus, E_A, E_B, E_C (GPa)	0.137, 210, 40
Poisson's ratio, ν_A, ν_B, ν_C	0.463, 0.275, 0.2

All numerical computations were performed using the software MATLAB. The plots are given in terms of frequency in Hz versus the reduced Bloch wave vector, i.e.,

$\bar{k}$=ka/2π. In the course of numerical calculations, 289 plane waves were considered for Fourier series expansion. In Fig. 4a, we illustrate the band structure for a homogeneous concrete thin plate without periodic inclusions, regarding square lattice. One can observe that there is no band gap opened up, neither Bragg-type nor resonance-type, since that both Bragg scattering and local resonance mechanisms were not present. In Fig. 4b, periodic circular steel inclusions with no coating are embedded in the concrete matrix, i.e., a PnC is regarded, called phononic concrete. The band structure was calculated considering square lattice, $\bar{f}_i$=0.335 and the other physical parameters of Table I. It can be observed the presence of two partial Bragg-type band gaps (represented by black shaded regions). The Bragg-type band gaps can be extended to the entire FBZ or not, whether not they are known as partial (or directional) Bragg-type band gaps. In Fig. 4, plots are limited until 132000 Hz.

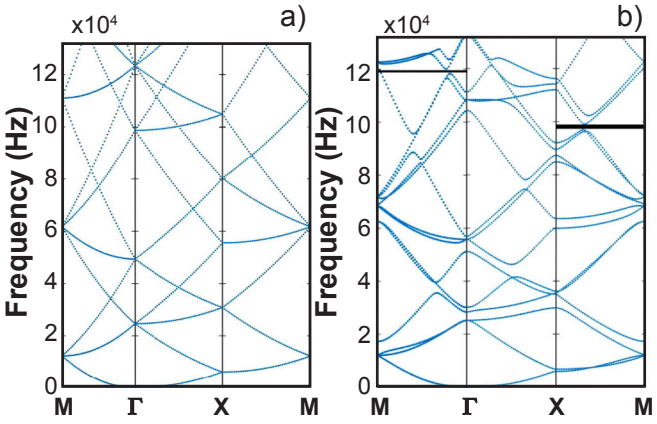

Figure 4: Elastic band structures of the concrete thin plate (a) and phononic concrete thin plate composed of a concrete matrix with circular steel inclusions (b), considering square lattice.

Fig. 5a illustrates the band structure for a homogeneous concrete thin plate without periodic inclusions, regarding triangular lattice. Similar as Fig. 4a, there is no band gap opened up in Fig. 5a, as explained before. In Fig. 5b, the band structure of a phononic concrete with triangular lattice and circular steel inclusions was calculated considering $\bar{f}_i$=0.335 and the other physical parameters of Table I. Plots are limited until 132000 Hz. One can observe the presence of five partial Bragg-type band gaps. This behavior was better than that observed for the square lattice in Fig. 4b, since more Bragg-type band gaps were opened up. Furthermore, some of these band gaps were broader for triangular lattice, Fig. 5b, and were created in lower frequencies.

From now on, we address the main case of this study, which is the metaconcrete thin plate (see Figs. 6 and 7). The elastic band structure was calculated using the fixed filling fractions described in Table I for the three inclusion cross-section geometries illustrated in Fig. 3, i.e., the thickness of the rubber coat and the steel core size did not vary. The influence of the thickness of the rubber coat was reported in [28]. In order to verify that the metaconcrete thin plate had both types of band gaps, i.e., local resonant

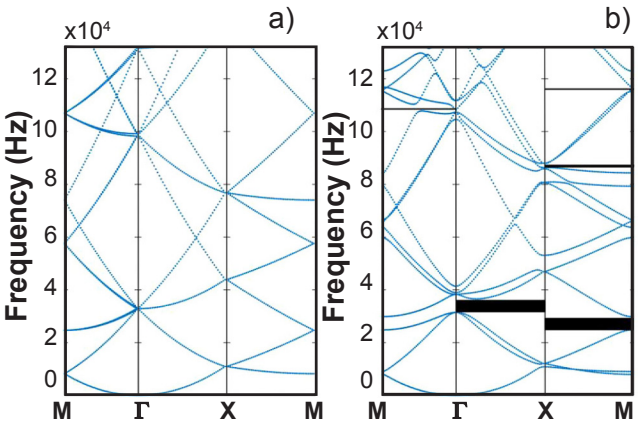

Figure 5: Elastic band structures of the concrete thin plate (a) and PnC thin plate composed of a concrete matrix with steel inclusions (b), considering triangular lattice and circular inclusions.

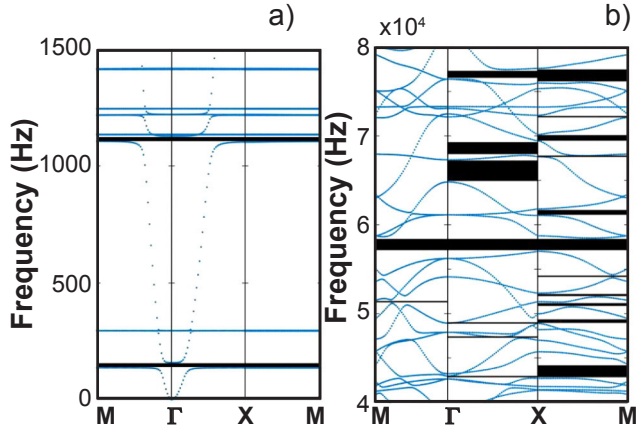

Figure 6: Elastic band structure of the metaconcrete thin plate with circular steel inclusions coated by rubber, considering square lattice, for low (a) and high (b) frequencies.

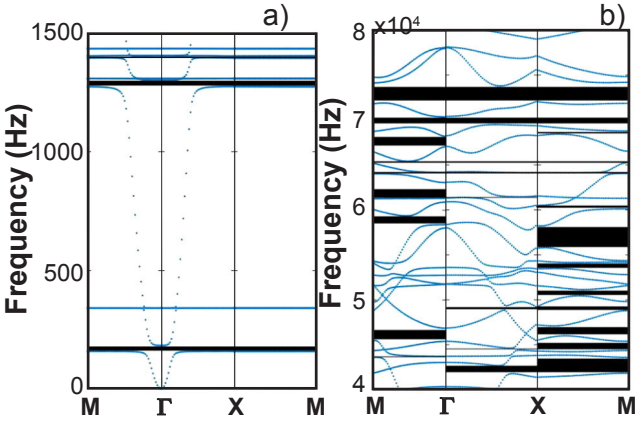

Figure 7: Elastic band structure of the metaconcrete thin plate with circular steel inclusions coated by rubber, considering triangular lattice, for low (a) and high (b) frequencies.

and Bragg-type, we illustrate in Figs. 6 and 7 its band structure with the LRBGs (a) and Bragg-type band gaps (b), regarding circular inclusions and square and triangular lattices, respectively. The metaconcrete thin plate with triangular lattice (Fig. 7b) showed more partial and

complete Bragg-type band gaps than square lattice (Fig. 6b) until 80000 Hz, considering circular inclusions. Otherwise, a broad complete Bragg-type band gap was observed for a square lattice in lower frequencies (near 60000 Hz) than in a triangular lattice.

Hereafter, only the LRBGs were studied, since they are the spotlights of this investigation. The band structure plots were limited until 1500 Hz. Fig. 8 illustrates the band structure of the metaconcrete thin plate with square lattice for circular (a), square (b) and rotated square (c) inclusions. There are two LRBGs regarding all inclusions in Fig. 8. The first LRBG for circular (a), square (b) and rotated square (c) inclusions in a square lattice had the following band gap width (midgap frequency): 21.6 (147.85), 24.8 (170.7) and 24.6 Hz (169.5 Hz), respectively. The band gap width was calculated by means of the difference between the higher and lower edge frequencies of the band gap. Both band gap width and midgap frequency are normally reported in band structure analysis [30]. Moreover, for the second LRBG, considering circular (a), square (b) and rotated square (c) inclusions in a square lattice, one had the following band gap width (midgap frequency): 23 (1116.5), 23 (1180.5) and 21 Hz (1149.5 Hz), respectively. One can observe that the widths of these two LRBGs for circular, square and rotated square inclusions were similar. In addition, the LRBGs for square and rotated square inclusions were slightly shifted to higher frequencies than that given by circular inclusion.

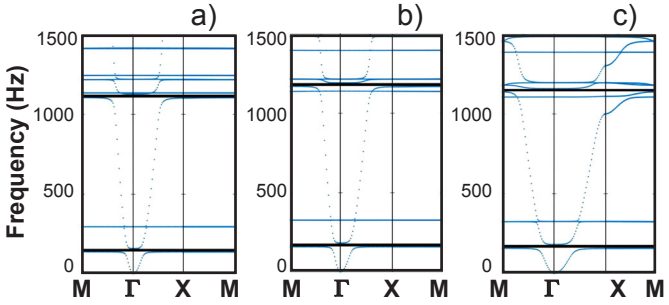

Figure 8: Elastic band structure of the metaconcrete thin plate with square lattice, considering circular (a), square (b) and rotated square with a 45° angle of rotation with respect to the x, y axes (c).

The elastic band structure is a result of the interaction of dispersion curves of high-velocity bulk waves in the matrix (concrete) with the low-frequency resonances of the circular, square and rotated square inclusions [19]. The LRBGs observed in Fig. 8 are related to the low stiffness of the rubber which results in low-frequency resonances [19]. Rubber is a very weak material, which allows the steel to vibrate within its coating, thus, the sound attenuating frequency bands are not determined by the scatter's distribution, but by their intrinsic structure [29]. The formation of LRBGs and the mechanism of flat bands have already been discussed in detail for a 2D ternary LRPnC with square lattice [31]. Wang and co-workers [31] studied the first four in-plane modes (XY modes) at the four flat bands and the first two out-of-plane modes (Z modes) of the first two flat bands. Flat bands, also known as flat branches [31], are frequency regions of no dispersion in the band structure, which correspond to localized modes [32], such as the ones at the Γ point in Fig. 8, and modes that also present zero group velocity, which also have a localized pattern. Flat bands that were not excited by an incident wave in the concrete matrix corresponded to localized modes in the rubber due to its low speeds.

The flat bands that cross the entire FBZ are also resonant modes [19]. However, these localized resonant modes did not open up any LRBG. This feature can be explained with the rule concluded in the binary case [33] (i.e., binary LRPnC) and used to judge whether a resonant mode can result in a corresponding sub-frequency band gap [31]. In addition, the LRBGs in a metamaterial appear even in the absence of periodicity [33]. Sometimes, the flat bands have more than one mode at the same frequency, i.e., degenerate modes, for instance, the tangential degeneracy [34, 35] observed in [31] for the in-plane modes. In Fig. 8a, one may observe some flat bands at 295.3 (first flat band), 1134, 1136, 1218, 1220, 1245, 1246, 1413 and 1417 Hz. Note that some frequencies of the flat bands were very close, which suggested that this slight difference was associated with IPWE simulation. Theoretically, two degenerate modes must have identical frequencies with different spatial patterns. However, slightly different frequencies can be found in numerical approaches. Thus, some close frequencies were associated with the same flat band, i.e., 1134 and 1136 Hz (second flat band), 1218 and 1220 Hz (third flat band), 1245 and 1246 Hz (fourth flat band), and 1413 and 1417 Hz (fifth flat band). In this study, we did not investigate the spatial pattern of these flat bands and hereafter only the LRBGs are analyzed.

In Fig. 9, we illustrate the band structure of the metaconcrete thin plate with triangular lattice for circular (a), square (b) and rotated square (c) inclusions. Three LRBGs were opened up for circular (a) and rotated square (c) inclusions, whereas four LRBGs were created considering square (b) inclusions. The first LRBG for circular (a), square (b) and rotated square (c) inclusions in a triangular lattice had the following band gap width (midgap frequency): 25.2 (170.7), 28.5 (196.35) and 28.5 Hz (195.95 Hz), respectively. The second LRBG had 34 (1292), 4 (1279) and 3 Hz (1277.5 Hz) of band gap width (midgap frequency), respectively, considering circular (a), square (b) and rotated square (c) inclusions. Moreover, the third LRBG presented 11 (1401.5), 21 (1356.5) and 24 Hz (1339 Hz) of band gap width (midgap frequency), respectively, considering circular (a), square (b) and rotated square (c) inclusions. The fourth LRBG was opened up only for square inclusions (c) and it had a band gap width (midgap frequency) of 3 Hz (1422.5 Hz). The first three LRBGs for square and rotated square inclusions presented similar behavior. However, a fourth narrow LRBG was created considering rotated square inclusions. The widths of the first LRBG for circular, square and rotated square inclusions were similar. However, for the second LRBG, narrow band gap widths were observed for square and rotated square inclusions in Figs. 9b and 9c, respectively. Furthermore, similar to the square lattice (Fig.

8), the first LRBG for square and rotated square inclusions were slightly shifted to higher frequencies than that given by circular inclusion, considering triangular lattice. Comparing the first two LRBGs observed for square (Fig. 8) and triangular (Fig. 9) lattices with circular (a), square (b) and rotated square (c) inclusions, we remark that circular inclusions presented broader LRBGs for triangular lattice. For square and rotated square inclusions, the width of the first LRBG was larger for triangular lattice, whereas the width of the second LRBG for these inclusions was larger for square lattice. The LRBGs for all inclusions in a triangular lattice were slightly shifted to higher frequencies than that given by square lattice. In addition, more LRBGs were opened up for triangular lattice.

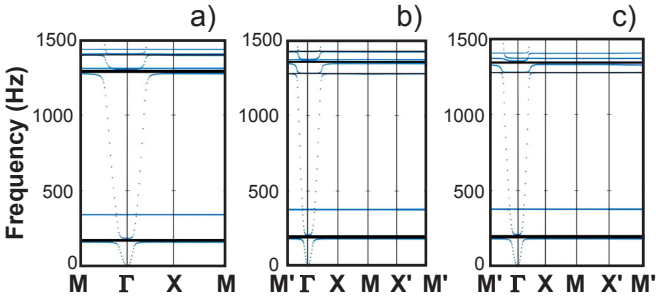

Figure 9: Elastic band structure of the metaconcrete thin plate with triangular lattice, considering circular (a), square (b) and rotated square with a 45° angle of rotation with respect to the x, y axes (c).

CONCLUSIONS

The elastic band structure of a metaconcrete thin plate with circular, square and rotated square inclusions in square and triangular lattices was investigated. The inclusions were composed by a steel core coated by rubber and they were periodically embedded in a concrete matrix. IPWE approach was formulated in order to find the real values of the Bloch wave vector, i.e., propagating Bloch waves. Kirchhoff-Love thin plate theory and flexural vibration were considered for band structure calculation. In addition, we did not study the influence of the thickness of the rubber coat and the steel core size for band gap formation. We first investigated the band structures of homogeneous concrete and phononic concrete thin plates with circular steel inclusions for both square and triangular lattices. In the first case, only Bragg-type band gaps were opened up. The best behavior until 132000 Hz was observed for triangular lattice, since broader partial Bragg-type band gaps were opened up in lower frequencies. After that, we calculated the band structures of a metaconcrete thin plate with circular steel inclusions coated by rubber for square and triangular lattices. We reported the presence of both LRBGs in low frequencies (until 1500 Hz) and Bragg-type band gaps in high frequencies (between 40 and 80 kHz). In this case, complete and partial Bragg-type band gaps were created for both lattices. We compared the band structures of the metaconcrete thin plate with circular, square and rotated square inclusions for square and triangular lattices. We showed the presence of flat bands that crossed the entire FBZ, which were localized resonant modes and did not open up LRBGs. More LRBGs were opened up for triangular lattice. However, some of them were narrower than for square lattice. Furthermore, for triangular lattice, the LRBGs for square and rotated square inclusions were slightly shifted to higher frequencies than that given by circular inclusion. In a general way, the band gap width and midgap frequency were subtly affected by inclusion geometry and by the lattice. Finally, we suggest that LRBGs in metaconcrete thin plates enlarge the potential applications for vibration management in low frequencies.

ACKNOWLEDGMENTS

The authors gratefully acknowledge FAPEMA and CAPES for their financial support of this investigation.

REFERENCES

[1] R.H. Olsson III, I. El-Kady, Meas. Sci. Technol. **20**, 1 (2009) 12002.
[2] Z. Liu, X. Zhang, Y. Mao, Y.Y. Zhu, Z. Yang, C.T. Chan, P. Sheng, Science **289**, 5485 (2000) 1734.
[3] C. Lv, D. Krishnaraju, G. Konjevod, H. Yu, H. Jiang, Sci. Rep. **4**, 5979 (2014) 1.
[4] Z. Chen, B. Guo, Y. Yang, C. Cheng, Physica B **438** (2014) 1.
[5] C. Lagarrigue, J. Groby, V. Tournat, J. Acoust. Soc. Am. **133**, 1 (2013) 247.
[6] Z. Yang, M.H. Dai, N.H. Chan, G.C. Ma, Appl. Phys. Lett. **96**, 4 (2010) 41906.
[7] F. Casadei, B.S. Beck, K.A. Cunefare, M. Ruzzene, J. Intell. Mater. Syst. Struct. **23**, 10 (2012) 1169.
[8] Z. Cheng, Z. Shi, Y.L. Mo, H. Xiang, J. Appl. Phys. **114**, 3 (2013) 33532.
[9] Z. Cheng, Z. Shi, Constr. Build. Mater. **50** (2014) 257.
[10] S.J. Mitchell, A. Pandolfi, M. Ortiz, J. Mech. Phys. Solids **65** (2014) 69.
[11] S.J. Mitchell, A. Pandolfi, M. Ortiz, Mech. Mater. **91** (2015) 295.
[12] S.J. Mitchell, A. Pandolfi, M. Ortiz, J. Eng. Mech. **142**, 4016010 (2016) 1.
[13] M. Miniaci, A. Krushynska, F. Bosia, N.M. Pugno, New J. Phys. **18**, 83041 (2016) 1.
[14] G. Kirchhoff, J. Reine Angew. Math. **40** (1850) 51.
[15] A.E.H. Love, Philos. Trans. R. Soc. **179** (1888) 491.
[16] L. Li, J. Opt. Soc. Am. A **13**, 9 (1996) 1870.
[17] Y. Cao, Z. Hou, Y. Liu, Phys. Lett. A **327**, 2-3 (2004) 247.
[18] L. Brillouin, *Wave propagation in periodic structures*, Dover Publ., New York (1946).
[19] J.-C. Hsu, T.-T. Wu, Jpn. J. Appl. Phys. **49**, 7S (2010) 7HB11.
[20] M.M. Sigalas, E.N. Economou, J. Appl. Phys. **75**, 6 (1994) 2845.
[21] F. Fahy, P. Gardonio, *Sound and structural vibration:*

radiation, transmission and response, Acad. Press (2007).
[22] Z.-J. Yao, G.-L. Yu, Y.-S. Wang, Z.-F. Shi, Int. J. Solids Struct. **46**, 13 (2009) 2571.
[23] G. Floquet, Ann. Sci. Ecole Norm. S. **12** (1883) 47.
[24] F. Bloch, Z. Phys. **52** (1928) 550.
[25] E.J.P. Miranda Jr., J.M.C. Dos Santos, Mat. Res. **20**, 2 (2017) 555.
[26] D. Qian, Z. Shi, Phys. Lett. A **381** (2017) 1516.
[27] E.J.P. Miranda Jr., J.M.C. Dos Santos, Mech. Syst. Signal Process. **112** (2018) 280.
[28] Z.-J. Yao, G.-L. Yu, J.-B. Li, Mater. Sci. Forum **675-677** (2011) 1085.
[29] M. Hirsekorn, P.P. Delsanto, N.K. Batra, P. Matic, Ultrasonics **42**, 1-9 (2004) 231.
[30] F. Wu, Z. Hou, Z. Liu, Y. Liu, Solid State Commun. **123**, 5 (2002) 239.
[31] G. Wang, Y.-Z. Liu, J.-H. Wen, D.-L. Yu, Chinese Phys. **15**, 2 (2006) 407.
[32] C. Goffaux, J. Sánchez-Dehesa, A.L. Yeyati, P.H. Lambin, A. Khelif, J.O. Vasseur, B. Djafari-Rouhani, Phys. Rev. Lett. **88**, 22 (2002) 225502.
[33] G. Wang, X. Wen, J. Wen, L. Shao, Y. Liu, Phys. Rev. Lett. **93**, 15 (2004) 154302.
[34] A.N. Darinskii, E. Le Clezio, G. Feuillard, Wave Motion **45**, 7-8 (2008) 970.
[35] A.G. Every, A.A. Maznev, W. Grill, M. Pluta, J.D. Comins, O.B. Wright, O. Matsuda, W. Sachse, J.P. Wolfe, Wave Motion **50**, 8 (2013) 1197.
(Rec. 30/08/2018, Ac. 01/11/2018)